Forced axial segregation in axially inhomogeneous rotating systems

S. González,[1] C. R. K.Windows-Yule,[2,*] S. Luding,[1] D. J. Parker,[2] and A. R. Thornton[1,3]
[1]*Multi-Scale Mechanics, Department of Mechanical Engineering, MESA+, University of Twente, P.O. Box 217, 7500 AE Enschede, The Netherlands*
[2]*School of Physics and Astronomy, University of Birmingham, United Kingdom, B15 2TT*
[3]*Mathematics of Computational Science, Department of Applied Mathematics, MESA+, University of Twente, P.O. Box 217, 7500 AE Enschede, The Netherlands*
(Received 14 May 2015; published 4 August 2015)

Controlling segregation is both a practical and a theoretical challenge. Using a novel drum design comprising concave and convex geometry, we explore, through the application of both discrete particle simulations and positron emission particle tracking, a means by which radial size segregation may be used to drive axial segregation, resulting in an order of magnitude increase in the rate of separation. The inhomogeneous drum geometry explored also allows the direction of axial segregation within a binary granular bed to be controlled, with a stable, two-band segregation pattern being reliably and reproducibly imposed on the bed for a variety of differing system parameters. This strong banding is observed to persist even in systems that are highly constrained in the axial direction, where such segregation would not normally occur. These findings, and the explanations provided of their underlying mechanisms, could lead to radical new designs for a broad range of particle processing applications but also may potentially prove useful for medical and microflow applications.

DOI: 10.1103/PhysRevE.92.022202 PACS number(s): 81.05.Rm, 45.70.Mg

I. INTRODUCTION

Granular flows in rotating drums are widely used to study mixing, segregation, and pattern formation [1]. While most studies focus on a circular cylinder geometry, several recent works have explored different drum geometries [2–8], including asymmetric configurations [9]. Noncircular drums are important from both an application perspective, as they are used in various industries, and from a theoretical perspective, to further validate and develop theoretical approaches developed primarily from simpler cylindrical configurations. Segregation is known to occur in rotated drums containing granular materials; species-separation in the *radial* direction occurs after a few rotations [2]. Additionally, for adequately long drums, if rotation continues for a suitably large period of time (typically of the order of hundreds of drum rotations), *axial* segregation may also appear [10,11]. Even after the initial axial separation of the system, the segregated bands of differing particle species produced are known to often be metastable [12] and their positions irreproducible in repeated runs [13,14]. This raises two interesting questions: how can we accelerate axial segregation, and how can we produce stable, reproducible regions of segregated particles?

The role of geometry in segregation is well known [15], with experiments looking at a variety of convex [5,16–20] and concave [7,21–23] drums, including geometries commonly used in industry, such as the double-cone and V-blender [24–26]. In particular, work by McCarthy *et al.* [9] provides a detailed overview of the effects of system geometry on *radial* segregation, considering both simple polygonal and complex, nonconvex tumbler geometries. Work by Hill *et al.* [27] also demonstrates the important influence of system shape on segregation, focusing on the competition between order and the chaos induced by the introduction of noncircular geometries. This study also provides valuable insights into the origins of segregation in the *axial* direction, demonstrating its presence in noncircular systems, even in the absence of a radial core, which had previously been suggested to be a necessary precursor to axial segregation [11].

However, to the best of our knowledge this current work provides the first investigation of mixed convex-concave systems. In geometry concave polygons are defined by two numbers $\{n/m\}$; n is the number of sides (points on a circle) and the polygon is formed by connecting every mth point with straight lines. We chose the simplest regular concave polygon the $\{5/2\}$-star polygon, or pentagram. In this paper, we first focus on the dynamics of monosized particles in simple concave drums and later explain how the novel combination of concave and convex shapes can be used to accelerate axial segregation and even deliberately impose specific segregation patterns on a system.

II. EXPERIMENTAL DETAILS

A. Setup

Drums of fixed size $D = 119$ mm (with D the diameter of the circle in which all polygons investigated are inscribed) and width $\Delta z \in (10,24)$ mm are partially filled with glass beads of diameter $d = 3.5 \pm 0.3$ mm and rotated at a constant rate $\Omega = \pi/2$ rad/s. The coordinate system used within this article is defined such that the z axis lies parallel to the drum's axis of rotation and perpendicular to the direction of gravity (i.e., the drum is not inclined), the y axis lies in the vertical direction opposing gravity and the x axis lies perpendicular to the z and y axes.

B. Positron emission particle tracking

Data is acquired from the experimental system using both optical techniques and positron emission particle tracking (PEPT), enabling the bed's exterior and interior to be explored.

*c.r.windows-yule@utwente.nl

PEPT is a nonintrusive technique that records the motion of a single "tracer" particle in order to extrapolate of a variety of time-averaged quantities pertaining to the system as a whole. In order to perform PEPT, a single particle—physically identical to others of its species—is irradiated with a ^{3}He beam from the Birmingham cyclotron, producing β^+ activity within the tracer. The annihilation of the positrons emitted with electrons within the tracer medium produces, due to conservation of momentum, a pair of 511 keV γ rays whose trajectories are separated by 180°. The straight-line trajectories of these γ photons, when detected simultaneously by the two detectors of a dual-headed positron camera (a "coincidence event"), allow their path to be reconstructed. Thus, by detecting multiple γ-ray pairs, the position of the tracer particle can be triangulated to submillimeter accuracy in three-dimensional space. For adequately active particles, the high rate of coincidence events allows particle motion to be tracked with a temporal resolution on the millisecond scale. Moreover, the use of energetic, highly penetrating γ rays allows particle motion to be tracked and recorded even deep within the bulk of large, dense, and/or opaque systems.

For systems in an ergodic steady state, the single-particle motion recorded using PEPT can, through the use of appropriate time averages [28], be used to acquire a variety of whole-field quantities, such as one-, two-, or three-dimensional packing density and granular temperature fields [29], velocity vector fields [30,31], convection strength [32], or for bi- and polydisperse systems, segregation intensities [33] and concentration fields [34]. For a steady-state system such as ours, the fractional residence time, τ^f, of the tracer in any given region of the experimental volume is directly proportional to the time-averaged local packing density within the same region [28]. Thus, for a two-component granular bed, by subdividing the experimental system into a series of equally sized, three-dimensional voxels and comparing the residence time of a single particle of each constituent within a given pixel, the time-averaged local fractional concentration of each species can be simply determined as $\phi_1 = \frac{\tau_1^f}{\tau_1^f + \tau_2^f}$, where the indices 1 and 2 represent differing particle species. By performing this calculation for each voxel and then depth-averaging through a given spatial dimension, concentration plots such as those shown in Figs. 4 and 5 may be produced. In a similar manner, by averaging the velocities of all transits made by a tracer particle through a given voxel, one may produce two-dimensional velocity vector fields such as those presented in Fig. 6. Although not necessary to the understanding of this paper, for the interested reader, a more comprehensive overview of the PEPT technique may be found in our reference [35], while a proof of the equivalence between time-averaged single-particle data and ensemble-averaged whole-field data is presented in Ref. [28].

III. SIMULATIONS

Simulations are performed using the MercuryDPM software package [36–39] developed at the University of Twente. In simulations, experimental system dimensions and particle properties are used. We simulate a collection of bidispersed spherical particles of different diameters d_s and d_l, with the same density ρ; each particle i has a position $\boldsymbol{r}_i$, velocity $\boldsymbol{v}_i$, and angular velocity $\boldsymbol{\omega}_i$. It is assumed that particles are spherical, soft, and the contacts are treated as occurring at single points. The relative distance between two particles i and j is $r_{ij} = |\boldsymbol{r}_i - \boldsymbol{r}_j|$, the branch vector (the vector from the center of the particle to the contact point) is $\boldsymbol{b}_{ij} = -(d_i - \delta_{ij}^n)\hat{\boldsymbol{n}}_{ij}/2$, the unit normal is $\hat{\boldsymbol{n}}_{ij} = (\boldsymbol{r}_i - \boldsymbol{r}_j)/r_{ij}$, and the relative velocity is $\boldsymbol{v}_{ij} = \boldsymbol{v}_i - \boldsymbol{v}_j$. Two particles are in contact if their overlap,

$$\delta_{ij}^n = \max[0,(d_i + d_j)/2 - r_{ij}],$$

is positive. The normal and tangential relative velocities at the contact point are given by

$$\boldsymbol{v}_{ij}^n = (\boldsymbol{v}_{ij} \cdot \hat{\boldsymbol{n}}_{ij})\hat{\boldsymbol{n}}_{ij} \tag{1}$$

and

$$\boldsymbol{v}_{ij}^t = \boldsymbol{v}_{ij} - (\boldsymbol{v}_{ij} \cdot \hat{\boldsymbol{n}}_{ij})\hat{\boldsymbol{n}}_{ij} + \boldsymbol{\omega}_i \times \boldsymbol{b}_{ij} - \boldsymbol{\omega}_j \times \boldsymbol{b}_{ji}. \tag{2}$$

Particles are assumed to be linearly viscoelastic; therefore, the normal and tangential forces are modeled as a spring-dashpot with a linear elastic and a linear dissipative contribution [40,41]. Hence, the normal and tangential forces, acting from j on i, are given by

$$\boldsymbol{f}_{ij}^n = k^n \delta_{ij}^n \hat{\boldsymbol{n}}_{ij} - \gamma^n \boldsymbol{v}_{ij}^n, \quad \boldsymbol{f}_{ij}^t = -k^t \boldsymbol{\delta}_{ij}^t - \gamma^t \boldsymbol{v}_{ij}^t, \tag{3}$$

where k^n and k^t are the spring constants and γ^n and γ^t are the damping constants. The elastic tangential displacement, $\boldsymbol{\delta}_{ij}^t$, is defined to be zero at the initial time of contact, and its evolution is given by

$$\frac{d}{dt}\boldsymbol{\delta}_{ij}^t = \boldsymbol{v}_{ij}^t - r_{ij}^{-2}\left(\boldsymbol{\delta}_{ij}^t \cdot \boldsymbol{v}_{ij}\right)\boldsymbol{r}_{ij}, \tag{4}$$

where the second term corrects for the rotation of the contact, so that $\boldsymbol{\delta}_{ij}^t \cdot \hat{\boldsymbol{n}}_{ij} = 0$. When the tangential to normal force ratio becomes larger than the microscopic friction coefficient, μ, the tangential spring yields and the particles slide, truncating the magnitude of $\boldsymbol{\delta}_{ij}^t$ as necessary to satisfy $|\boldsymbol{f}_{ij}^t| < \mu|\boldsymbol{f}_{ij}^n|$. Specifically, normal and tangential spring constants $k_n = 100\,\mathrm{Nm}^{-1}$ and $k_t = \frac{2}{7}k_n$ are used, while the corresponding damping coefficients are taken as $\gamma_n = \gamma_t = 0.002\,\mathrm{s}^{-1}$, such that the frequency of normal and tangential contact oscillations, and the normal and tangential dissipation are equal. The microscopic friction coefficient is set to $\mu = 1$. A more detailed description of the contact law used can be found in Weinhart *et al.* [42] and for a detailed discussion of contact laws, in general, we refer the reader to the review by Luding [41]. The total force on particle i is a combination of the contact forces $\boldsymbol{f}_{ij}^n + \boldsymbol{f}_{ij}^t$ between all particle pairs i, j, currently in contact, and external forces, which for this investigation will be limited to only gravity. We integrate the resulting force and torque relations in time using Velocity-Verlet [43] and forward Euler with a time step $\Delta t = t_c/50$, where t_c is the contact duration for a head-on collision, which is given by

$$t_c = \pi \Bigg/ \sqrt{\frac{k^n}{m_{ij}} - \left(\frac{\gamma^n}{2m_{ij}}\right)^2}, \tag{5}$$

where $m_{ij} = m_i m_j/(m_i + m_j)$ is the reduced mass [41].

The drum rotation is achieved by changing the direction of gravity at fixed angular velocity $\Omega = \pi/2$ rad/s in order to

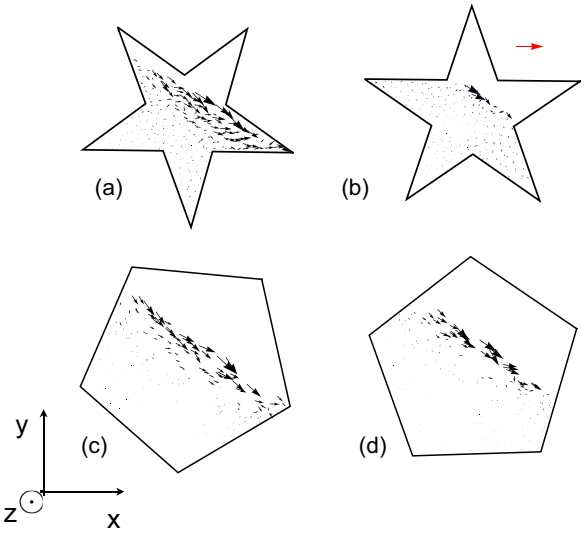

FIG. 1. (Color online) Simulation data showing instantaneous velocity fields for $F = 60\%$, $\Delta z = 10$ mm. Arrows represent velocity, v, projected on the x-y plane for all particles. The horizontal arrow in the top-right panel represents 0.25 ms^{-1}. The velocity vectors shown corresponds to a single "snapshot" of the system, each arrow representing the velocity of a given particle within the system.

consistently provide a continuous free-surface avalanche [44]. Simulations are conducted with periodic boundary conditions in the axial direction, as well as with rigid "end walls" allowing both direct comparison with experimental results in the case of the convex-concave (pentagon-pentagram) drum, and investigation of the effect of drum geometry on flow for purely convex or concave systems using periodic walls. Specifically, the data presented in Figs. 1 and 2 and discussion relating to simulations of homogenously convex and/or concave drums correspond, unless specifically stated otherwise, to data acquired using periodic boundary conditions. All other numerical results detailed in the article (including all discussion of simulated axially inhomogeneous systems) are, unless otherwise stated, derived from simulations in which solid end walls are implemented.

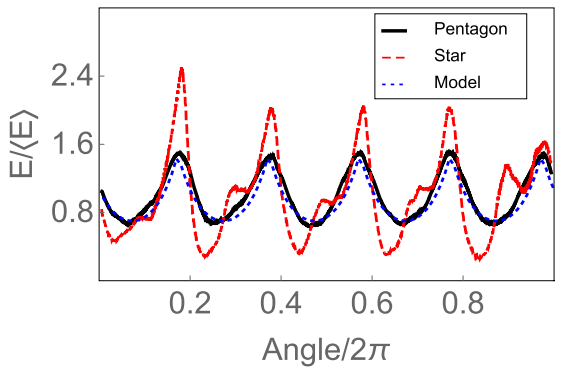

FIG. 2. (Color online) Kinetic energy vs. time during one cycle for a simulated (convex) pentagonal drum (solid, black), a (concave) pentagram (red, dashed), and the model for the pentagon (blue, dotted). Data averaged over 30 s of simulation taken 8 s after the start of the simulation.

IV. RESULTS AND ANALYSIS

A. The effect of the filling fraction

We observe four differing flow regimes depending on the filling fraction, F, defined as the fractional volume of the container occupied by grains. If grains occupy a volume smaller than one leg of the pentagram, they flow intermittently from leg to leg. If the F increases such that there are always grains in at least two legs, flow is constant but its angle changes continuously. When two to four legs are filled, flow is continuous but with two qualitatively different flow profiles depending on the drum's angle. Once grains occupy more than four legs, flow becomes intermittent and grain displacement is strongly limited, decreasing transport in the bulk, with dynamics mostly due to geometrical rearrangements. We focus on the regime $40\% \leqslant F \leqslant 60\%$, where unsteady flow is produced by a concave drum rotating at a constant rate. The geometric shape naturally causes periodic changes in the flowing layer as a function of the instantaneous orientation of the pentagram, as recently reported in other geometries [8].

B. Comparison of pentagram and pentagon

In cylindrical and general convex drums, steady flow has a roughly constant kinetic energy, $E = \sum \frac{1}{2} m_i v_i^2$, independent of the angle of rotation. For the pentagram, however, this oscillates strongly: when a pentagram points up, flow is slow, while when pointing down, flow is much faster. Figure 1 shows velocity fields for both pentagram [Figs. 1(a) and 1(b)] and pentagon [Figs. 1(c) and 1(d)]. The pentagram shows great variation in the magnitude of v between the up (b) and down configuration (a): when the pentagram points down, the avalanche occurs in a thick layer. As the drum rotates, more space becomes available, producing a saltating flow. This creates a fast avalanche in the down part of the flow, and the consequent movement of all the flowing layers. Thus, E shows five maxima during a cycle (Fig. 2). By allowing particles more space to flow, a large, fast avalanche is produced. This avalanche is not homogeneous along the free-surface. Most of the kinetic energy is on the downside, where the free volume makes it easier to flow. Eventually, the leg is filled with particles and the avalanche recovers its slow flow, before the process repeats. We now focus on how this feature can be used to control segregation. To do this, one must introduce the pentagram's convex counterpart, the pentagon. As the pentagon rotates, the total length of the flowing layer changes, creating an oscillation in E with the same period as for the pentagram (see Fig. 2). However, this flow, and its velocity, are much more consistent in the pentagon, with a smaller variation between minimum and maximum.

The periodic structure of the E can be understood by simple arguments. If one considers the speed of the flowing layer and its depth constant as much smaller than the filling height, H, then E is proportional to the length, L, of the flowing layer [8]. Disregarding the angle of the walls, and assuming a straight free surface, L scales approximately as $L \propto 1/\cos(\theta)$, with $\theta \in [0, 2\pi/5]$ the angle of rotation modulo the shape's symmetry, in this case $2\pi/5$. Hence, $E \propto 1/\cos(\theta)^2$, with $\theta = 0$ corresponding to the phase during the rotation for which the pentagon and pentagram are pointing directly upward. The

agreement of simulations with this simple model is remarkable (see Fig. 2), although deviations from this simple sinusoidal form arise for the concave drum. These deviations are not surprising, as in a pentagon the flowing layer is at the edge of the geometric region of constant volume and this region is always connected, giving a relatively consistent filling fraction, F, the same does not hold for pentagrams and other concave shapes. Consequently, both of the above assumptions are likely to be broken for such geometries. Specifically, one observes the presence of local maxima preceding each of the main peaks in kinetic energy. It is also notable that the first maximum in E is markedly higher than the following peaks. The former of these deviations can be explained by the fact that particles in the lower region of the surface flow avalanche first over the lowermost leg, before being followed by grains in the middle and upper regions, thus leading to the observed "two-part" increase in E [45]. The first increase in E, which only appears thanks to the geometry of the container, forms the basis of our discussion in the following section, where we demonstrate the manner in which an axial segregation whose speed is comparable to the radial one may be induced. The latter, meanwhile, can be explained by the presence of localized jamming within the system, whereby a collection of particles in a jammed state is able to reach a higher point in the system before avalanching, naturally resulting in a higher-than-average kinetic energy. It is finally worth noting that, for a uniformly concave geometry, the introduction of end walls acts to frustrate the smaller, local maxima in the energy, E, as the increased confinement reduces the system's ability to flow, thus causing the smaller first peak to simply merge with the larger second peak. Thus, while the general sinusoidal evolution of E is found to persist, the additional, localized peaks are eliminated; i.e., the concave system approaches more closely the theoretical form. For the case of a mixed concave-convex geometry, however, the initial flow corresponding to the first, local maxima is *not* suppressed, due to the presence of an additional free boundary at the interface between the regions of differing geometry.

C. Shape-induced axial segregation

Although the influence of a nonuniform container shape on segregation has already been reported [46,47], this is the first time, to our knowledge, that it is used in a rotating drum. It is also known that modifying the geometry of the tumbler (e.g., adding obstacles or mixing blades) can *eliminate* segregation [48] but it has not been shown how to *augment*, *accelerate*, and *direct* it—a matter of obvious practical importance. For bidisperse granulates in a rotating container, small particles will typically migrate toward the drum's center [1,49] [see Figs. 3(a) and 3(b)]. It should be noted, however, that, dependent on the specific geometry, rotation rate and fill height of the system in question, this is not always the case—previous studies have noted, under certain circumstances, differing radial segregation patterns [9,27]. For adequately wide systems, upon continuous rotation the system will segregate axially [10], a process approximately two orders of magnitude slower than radial segregation. However, if two different geometries are used along the axial direction, e.g., a half-pentagram, half-pentagon drum, the usually slow

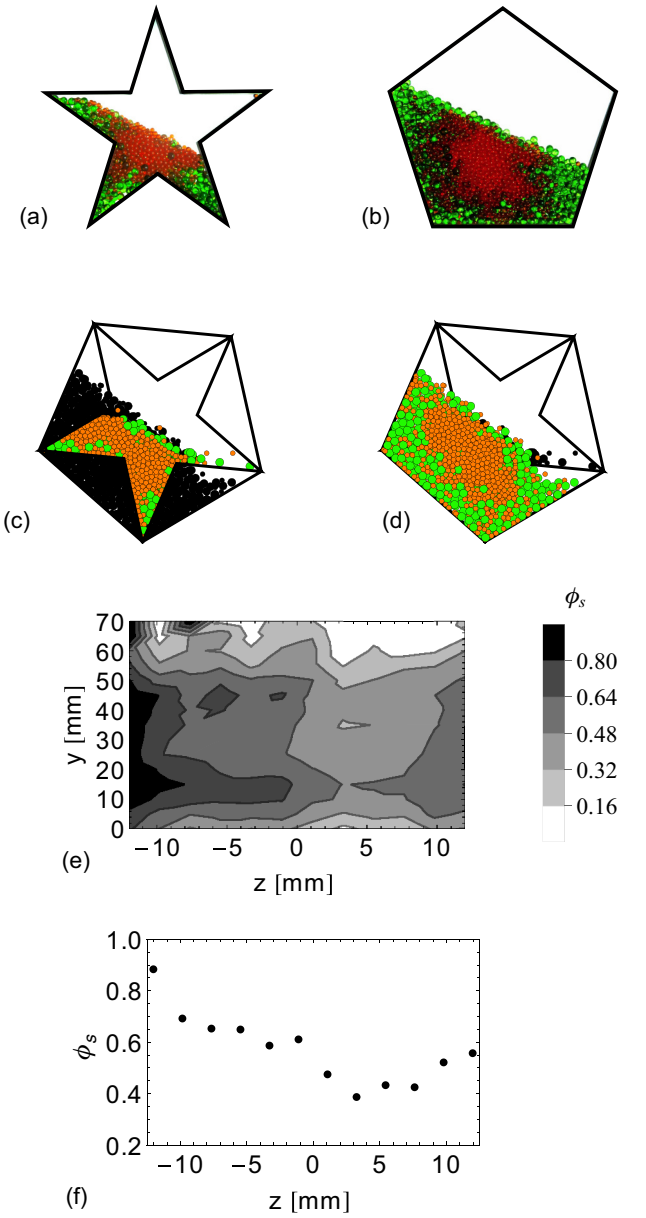

FIG. 3. (Color online) Photographs of the experiment after four revolutions in the axially homogeneous drum for (a) the pentagram and (b) the pentagon, each showing radial segregation. Simulations for the axially inhomogeneous, layered drum after four revolutions, from the pentagram-shaped side (c) and from the pentagonal side (d). Particles are colored by size with orange small and green large; black particles correspond to those particles that belong to the opposite side of the drum. Finally, time averaged spatial variation of the fractional concentration of small particles, ϕ_S, for a two-dimensional (2D) projection through the x axis (e), and as a 1D profile along the axial (z) direction (f). In both panels (e) and (f), negative z values correspond to the concave region of the drum and positive values correspond to the convex region. The data is averaged over 1000 individual snapshots spanning 8 s of simulation. The simulation results show a larger concentration of small particles close to the walls in both sides of the drum than the experimental results (see Fig. 5). We attribute this discrepancy to the fact that in the experimental setup there is considerably more noise than in the simulations. This noise will increase the diffusion in the system, and since the segregation is forced by the geometry, a moderate noise increases it.

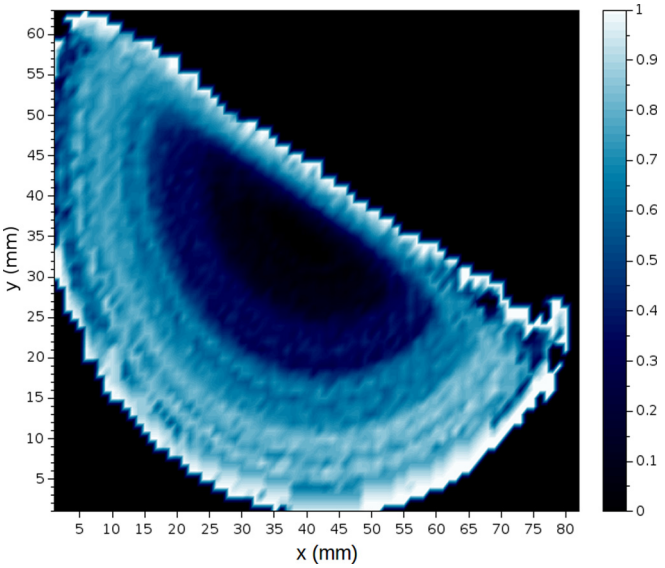

FIG. 4. (Color online) Spatial distribution in the x-y (radial) plane of the fractional concentration, ϕ_L, of large particles. The data shown are time-averaged over the duration of the run (τ_r = 7200 s) and depth-averaged through the axial direction across both concave (pentagram) and convex (pentagon) segments. Due to the time-averaged nature of the data presented, the specific geometry of the drum is not visible.

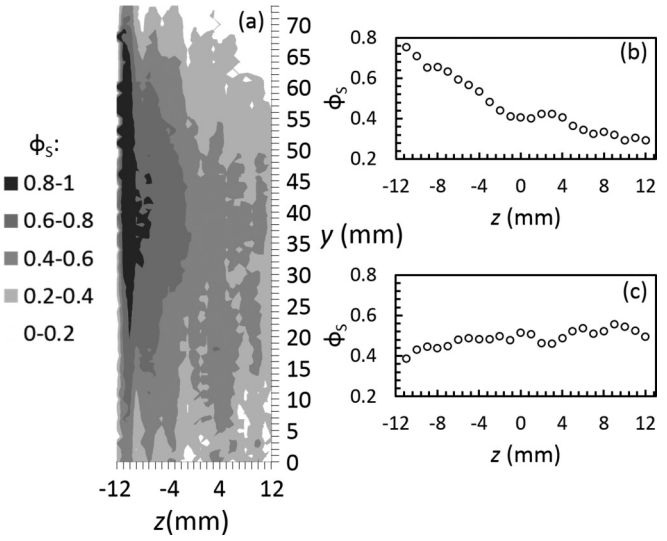

FIG. 5. Experimental data acquired using PEPT showing the time-averaged spatial variation of the fractional concentration of small particles, ϕ_S, for a two-dimensional (2D) projection through the x axis, and as a 1D profile along the axial (z) direction. In panels (a) and (b), negative z represents the concave, and positive z represents the convex sides of a pentagram-pentagon drum. Shown also is the 1D profile for an equivalent, purely convex system (c), illustrating the enhanced segregation produced by the dual-geometry system. In all cases, $F = 60\%$, $\Delta z = 24$ mm.

segregation along this axis can be enhanced and its direction controlled [see Figs. 3(c) and 3(d)]. Not only this, it is also possible to induce strong, two-band axial segregation even in extremely short systems [$\frac{\Delta z}{D}\mathcal{O}(0.1)$] where such banding would not normally occur. In both experiment and simulation, two sections of equal width are combined. We use particles of $d = 4.0, 2.5$ mm, in an equal volume distribution. The rapid axial segregation happens only with a convex-concave (pentagon-pentagram) combination, as for convex shapes there exists little difference in the level of the flow, just the length of avalanching layer [50]. We performed several experiments, putting together circular and square sections, pentagonal and square, and differently oriented square sections. None of these configurations presented axial segregation on the time scale of observation ($\sim$20 revolutions). A clearer representation of the segregation—both axial and radial—achieved in the convex-concave system described above may be seen in Figs. 3, 4, and 5. Figures 3(c) and 3(d) show the typical radial distribution of particles for a given instant in time, while Fig. 4 illustrates the *time-averaged* radial distribution of particles as acquired from experimental PEPT data. Figure 5 demonstrates the experimentally obtained *axial* distribution of small particles in both one and two dimensions. In all images shown, positive positions along the z axis represent the convex region of the drum, while negative z corresponds to the system's concave regions.

Grains tend to minimize their potential energy, i.e., move toward the concave side, which also possesses more free volume. Note that the few large grains in the run-out leg of Fig. 3(c) will eventually fall to the pentagonal side. Radial segregation occurs in each side, so large particles go to the surface and small particles go to the center. Since for this packing fraction the avalanche in the pentagonal side of the drum ($z > 0$) is slower than in the pentagram-shaped section ($z < 0$), large particles can move to the empty side since they are faster and there is space available for them. Once the two avalanches reach the same angle there is no more flux of particles. This process is repeated five times per revolution [see Fig. 7(a)]. When the big particles drop from the run-out leg of the pentagram to the pentagon, the center of mass of the large particles shifts toward the pentagon. However, the process is not completely irreversible; some, but fewer, large particles go again to the pentagram side as the drum rotates. In this way, an oscillating movement of the center of mass of each species is observed: big particles fall to the pentagonal side when the run-out leg is empty; once the flow covers the run-out leg some large particles return to the pentagram side. By this mechanism, there is a net transport of large particles to the convex (pentagon) side of the drum. Similarly, since the average volume fraction within the system remains constant, conservation of mass requires an opposing flow of small particles into the drum's concave region, leading to a preponderance of small particles in this region. This migration of particles will, naturally, result in a predominance of smaller particles in the concave section, and hence a relatively increased angle of repose in this region [51,52]. The slope produced between the two adjacent sections (clearly visible in Fig. 6) will lead to a cascade of larger particles from still deeper within the concave (pentagram) region into the convex region, thus further exacerbating the observed segregation. Since the above-described mechanism relies on radial segregation, which is typically achieved in $\mathcal{O}(1)$ rotation [2], it is orders of magnitude faster than the axial segregation previously reported

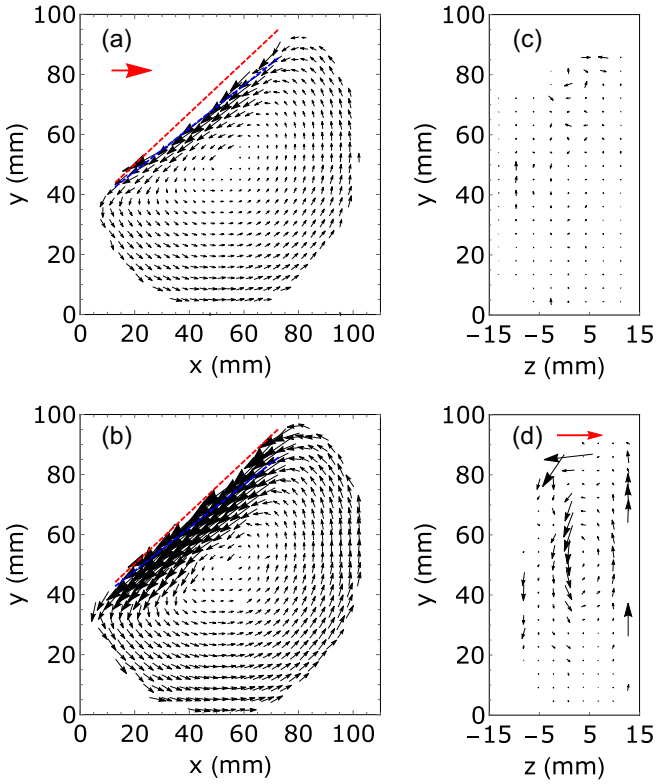

FIG. 6. (Color online) Time-averaged velocity fields for an experimental pentagram-pentagon system of width $\Delta z = 24$ mm. Panels (a) and (b) show, for the convex (pentagon) and concave (pentagram) regions, respectively, the radial velocities of particles in the cartesian x-y plane, where the x and y directions lie perpendicular to the axial z direction in the vertical (y) and horizontal (x) planes. Differences in angle between the free surfaces of the bed for the two regions are emphasized through the inclusion of a red dashed line corresponding to the concave region, and a blue dotted line representing the convex region. Panels (c) and (d) show depth-averaged particle flow in the z-y plane for small [panel (c)] and large [panel (d)] particles belonging to the same system. In all images presented, the direction and magnitude of the average particle velocity in a given region of the experimental volume are represented by the orientation and length of the arrows displayed. As with previous images, $z < 0$ corresponds to the drum's concave section and $z > 0$ corresponds to the convex region.

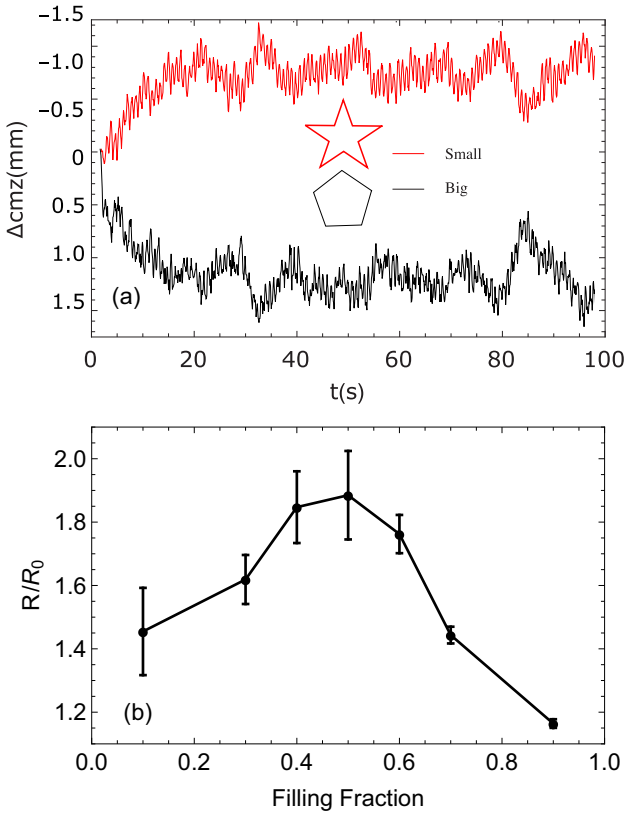

FIG. 7. (Color online) Top: evolution of the displacement of the center of mass for simulations at $F = 50\%$ in a pentagram-pentagon geometry of width $\Delta z = 22$ mm. The plot is produced by determining, for each individual snapshot, the center of mass for each species as $\frac{\sum m_i z_i}{\sum m_i}$, where m_i and z_i are, respectively, the mass and vertical position of the ith particle within the system. Bottom: Number ratio ($R = N_{\text{big}}/N_{\text{small}}$) in the pentagonal side of the drum ($z > 0$) versus the filling fraction normalized by the initial conditions. Data is averaged in ten snapshots during two turns of the drum. Error bars are the standard deviation of these measurements.

for axially homogeneous drums where banding appears only after $\mathcal{O}(100)$ revolutions [10].

Experimental evidence of the mechanism proposed above may be seen in Fig. 6. From these images it is clear that, as expected, there exists a difference in the level and angle of inclination of the bed's surface between the convex (pentagon) and concave (pentagram) sides of the drum. Moreover, the velocity fields in Figs. 6(a) and 6(b) demonstrate the avalanching region on the bed's concave side to be considerably faster than for the convex half, again in agreement with our hypothesis. Figures 6(c) and 6(d) show two-dimensional, depth-averaged velocity fields for the z-y plane, where y denotes a vertical axis perpendicular to the axial (z) axis. In Fig. 6(d), which corresponds to the time-averaged motion of the large particles in the system, we see evidence of the recirculatory transport discussed above, and whose effect on the system's mass center is shown in Fig. 7 (top panel). Note that such motion is seemingly absent for the small particles in the same system [Fig. 6(c)]. It should also be noted that while the circulatory motion of large particles is clearly visible from the time-averaged velocity vector fields presented, these fields cannot be expected to show the net migration of large (small) particles to the convex (concave) regions of the drum. The reasoning for this is that PEPT data is, in order to achieve good statistics, acquired from the steady-state of the system over a long duration. As such, the *net* flux of particles over this timescale will, naturally, be zero. In other words, while PEPT allows us to visualize the repeated, circulatory motion described above, which forms the *driving mechanism* underlying the observed segregation, the evolving segregation itself may only be observed from simulation.

In addition to the mechanism described above, there exists another possible driving force behind the segregation observed within the system. It was noted by Fan and Hill [53] that, for a circular split-bottom cell geometry, the presence of convective motion acted to advect large particles from upper

regions of their system downwards along one sidewall, and similarly carry small particles upwards along the opposing sidewall, thus creating a horizontal gradient in $\phi_{S,L}$. If the velocity field observed in Fig. 6(d) is instead interpreted to be evidence of a convection roll, it is possible that a similar process is acting within our own system. However, the authors doubt that such convective motion is in fact the origin of the behaviors observed here. First, unlike the system of Ref. [53], there exists no clear mechanism to explain the presence of convection within our system—indeed, the observed flow in our system more closely resembles that of the parallel split-bottom geometry for which Fan and Hill *do not* observe convection. Moreover, where Fan and Hill observe strong convective motion for both small and large species, the same cannot be said for our system [cf. Figs. 6(c) and 6(d)], once more implying that the circulatory motion observed does not correspond to convection.

A relevant test for our main hypothesis regarding the origin of the observed axial segregation, which, as stated above, is thought to be coupled to the existence of radial segregation, would be to see if the process persists in the absence of a clearly defined radial core. The use of noncircular systems such as ours have been repeatedly shown to induce chaotic behavior in the granular beds housed within [2,16,27,54] and thus to produce a variety of strongly differing radial segregation patterns. It is known [27] that certain combinations of geometry, filling fraction and rotation rate may indeed eliminate the simple radial core typically observed in rotated systems, meaning that such a test is certainly feasible, and, as such, is a worthy subject for future research.

Results obtained over a variety of differing filling fractions demonstrate that the final degree of segregation is not equal for every filling fraction, F. Figure 7 (bottom panel) shows the change in the number of large particles in the pentagonal side of the drum for different filling fractions. If F is too low, the avalanche on the pentagram side of the drum arrives concurrently with the one in the pentagon and axial segregation is slower. It should be noted that the first local maxima observed on the kinetic energy for the pentagram (Fig. 2) are the reason for these nonsimultaneous avalanches. One could argue that excluded volume effects make the small particles go preferably to the pentagram side since the big particles do not fit into the legs so easily, as reported in Ref. [47]. However, this mechanism alone does not explain the maximum in segregation at $\sim$50% filling fraction. The observed axial segregation is dependent on both the different flow height and the nonconcurrent avalanches in either side of the drum—without the presence of *both* of these factors, any segregation observed would occur on a considerably longer timescale. Each side of the drum has its own dynamics and geometry and when bringing a concave and convex section together, these interact to create a defined, rapidly achieved, and stable segregation pattern.

The stability of the segregation pattern produced by the mechanism described here is particularly notable, as axial segregation in circular geometries is typically observed to undergo a process of "coarsening" [55], whereby an initial, large number of thin, metastable bands gradually merge over a long period of time, eventually forming fewer, wider bands. In our system, the final, steady state is achieved without the intermediate steps, making our process not only quicker, but also more predictable and, importantly, reproducible.

It is finally worth noting the range of drum widths, Δz, for which results similar to those described in this paper may be expected. The simple, two-band segregation which forms the focus of the present work is found to persist for widths in the range $10 \leqslant \Delta z \leqslant 54$ mm. In fact, across this range, for a fixed filling fraction, rotation rate, and particle volume ratio, the strength of the observed segregation is found to be invariant of Δz, at least to within experimental error. The timescale on which the segregation occurs, meanwhile, is found to remain of the same order of magnitude (i.e., considerably faster than conventional axial segregation), although wider systems seemingly take slightly longer to achieve their equilibrium distribution; this small increase can likely be attributed to the greater number of particles that must migrate across the system, and the increased average distance over which these migrations occur. It is important to reiterate, however, that the difference in segregation rate is small [$\mathcal{O}(1)$ revolution slower between the fastest and slowest cases]; i.e., the observed segregation is still orders of magnitude faster than conventional axial segregation.

For $\Delta z > 54$ mm, the situation becomes significantly more complicated, as additional, competing segregative mechanisms emerge and, for $\Delta z \gg 54$, become dominant. Due to the complex phenomena observed within large Δz systems (and the fact that such systems are external to the main aims of the current study) we will not attempt to provide a full explanation of their behaviors here. However, certain key features of these wider systems *are* directly relevant to this work. First, the mechanism described in this paper is seemingly present for *all* drum lengths, Δz, although its effects are localized to the convex-concave (pentagon-pentagram) interface for wider systems.

Finally, preliminary results strongly suggest that the use of alternating concave and convex sections may allow the separation of arbitrarily wide systems to be controlled and accelerated. These matters will be discussed in detail in future publications.

V. CONCLUSION

In this paper we have studied granular flows inside the simplest possible regular concave drum, that is, a pentagramal geometry. Different regimes are found for a fixed angular velocity depending on the filling fraction. From intermittent avalanching (low filling fraction) to geometrical rearrangements (high filling) passing by continuous flow (intermediate filling). These flow patterns differ qualitatively from those observed in convex drums. We have used this insight to control the segregation of a binary granular system, achieving geometrically induced axial segregation orders of magnitude faster than previously reported. Moreover, we demonstrate the ability to deliberately and reliably induce a stable and predictable segregation pattern in a rotating granular system for a wide range of parameters, including the case of short drums, where strong axial separation is typically not observed.

The practical importance of this discovery can be far-reaching in industries ranging from pharmaceuticals to mining.

There exist several potential applications for our discovery, including, but by no means limited to, rotating kilns—allowing differential residence times depending on the size of the particles—and milling devices—whereby creating a sandwich of concave sections with a convex shape in the middle, large particles can be conducted into the middle of the mill, thus increasing efficiency by keeping the grinders and larger particles in the mill while moving the fines to the ends, where they could be removed. Our findings may even be used to provide a more efficient and, importantly, less environmentally damaging [56] manner by which to separate valuable materials from electronic waste—a process that is heavily reliant on strong segregation [57,58].

The mechanisms underlying the segregation observed are seemingly distinct from the relatively well-understood processes that may be modeled using continuum frameworks such as kinetic-sieving-style models [59–61] and adaptations such as the shear-induced segregation model [62,63]. The introduction of this mechanism provides scope for future work from a continuum-modeling perspective.

ACKNOWLEDGMENTS

We thank W. Zweers for the construction of the experimental setup, V. Ogarko for generating the bidisperse packings, and W. den Otter and N. Rivas for the critical reading of the article. This study was supported by the Stichting voor Fundamenteel Onderzoek der Materie (FOM), financially supported by the Nederlandse Organisatie voor Wetenschappelijk Onderzoek (NWO), through the FOM Project No. 07PGM27, and the Dutch Technology Foundation STW via Project No. 13472 STW, "Shaping-Segregation."

[1] G. Seiden and P. J. Thomas, Rev. Mod. Phys. **83**, 1323 (2011).
[2] K. M. Hill, N. Jain, and J. M. Ottino, Phys. Rev. E **64**, 011302 (2001).
[3] S. W. Meier, S. E. Cisar, R. M. Lueptow, and J. M. Ottino, Phys. Rev. E **74**, 031310 (2006).
[4] S. W. Meier, R. M. Lueptow, and J. M. Ottino, Adv. Phys. **56**, 757 (2007).
[5] L. Naji and R. Stannarius, Phys. Rev. E **79**, 031307 (2009).
[6] I. C. Christov, J. M. Ottino, and R. M. Lueptow, Chaos: Interdisc. J. Nonlin. Sci. **20**, 023102 (2010).
[7] D. V. N. Prasad and D. V. Khakhar, Phys. Fluids **22**, 103302 (2010).
[8] N. A. Pohlman and D. F. Paprocki, Jr., Granular Matter **15**, 1 (2012).
[9] J. J. McCarthy, T. Shinbrot, G. Metcalfe, J. E. Wolf, and J. M. Ottino, AIChE J. **42**, 3351 (1996).
[10] O. Zik, D. Levine, S. G. Lipson, S. Shtrikman, and J. Stavans, Phys. Rev. Lett. **73**, 644 (1994).
[11] K. M. Hill, A. Caprihan, and J. Kakalios, Phys. Rev. Lett. **78**, 50 (1997).
[12] N. Taberlet, W. Losert, and P. Richard, Europhys. Lett. **68**, 522 (2004).
[13] K. M. Hill and J. Kakalios, Phys. Rev. E **49**, R3610 (1994).
[14] K. M. Hill and J. Kakalios, Phys. Rev. E **52**, 4393 (1995).
[15] G. Metcalfe, T. Shinbrot, J. J. McCarthy, and J. M. Ottino, Nature **374**, 39 (1995).
[16] D. Khakhar, J. McCarthy, J. Gilchrist, and J. Ottino, Chaos: Interdisc. J. Nonlin. Sci. **9**, 195 (1999).
[17] J. J. McCarthy, D. V. Khakhar, and J. M. Ottino, Powder Technol. **109**, 72 (2000).
[18] N. Jain, J. M. Ottino, and R. M. Lueptow, Phys. Rev. E **71**, 051301 (2005).
[19] T. Kawaguchi, K. Tsutsumi, and Y. Tsuji, Particle Particle Syst. Character. **23**, 266 (2006).
[20] S. E. Cisar, J. M. Ottino, and R. M. Lueptow, AIChE J. **53**, 1151 (2007).
[21] P. W. Cleary, R. Morrisson, and S. Morrell, Int. J. Miner. Process. **68**, 129 (2003).
[22] D. Morton and S. Dunstall, Miner. Eng. **17**, 1199 (2004).
[23] A. Gupta, A. Katterfeld, B. Soeteman, and S. Luding, *World Congress Particle Technology 6, Nuremberg, CD Proceedings* (Nürnberg Messe GmbH, Nürnberg, 2010).
[24] M. Moakher, T. Shinbrot, and F. J. Muzzio, Powder Technol. **109**, 58 (2000).
[25] A. W. Alexander, T. Shinbrot, and F. J. Muzzio, Phys. Fluids **13**, 578 (2001).
[26] A. Alexander, F. Muzzio, and T. Shinbrot, Chem. Eng. Sci. **58**, 487 (2003).
[27] K. Hill, D. Khakhar, J. Gilchrist, J. McCarthy, and J. Ottino, Proc. Natl. Acad. Sci. U.S.A. **96**, 11701 (1999).
[28] R. D. Wildman, J. M. Huntley, J.-P. Hansen, D. J. Parker, and D. A. Allen, Phys. Rev. E **62**, 3826 (2000).
[29] R. D. Wildman, J. M. Huntley, and D. J. Parker, Phys. Rev. E **63**, 061311 (2001).
[30] R. D. Wildman, J. M. Huntley, and D. J. Parker, Phys. Rev. Lett. **86**, 3304 (2001).
[31] C. R. K. Windows-Yule, N. Rivas, D. J. Parker, and A. R. Thornton, Phys. Rev. E **90**, 062205 (2014).
[32] C. R. K. Windows-Yule, T. Weinhart, D. J. Parker, and A. R. Thornton, Phys. Rev. E **89**, 022202 (2014).
[33] C. R. K. Windows-Yule, T. Weinhart, D. J. Parker, and A. R. Thornton, Phys. Rev. Lett. **112**, 098001 (2014).
[34] K. Windows-Yule and D. Parker, KONA Powder and Particle J. **32**, 163 (2015).
[35] D. Parker, R. Forster, P. Fowles, and P. Takhar, Nucl. Instrum. Methods Phys. Res. A: Accel. Spectrom. Detect. Assoc. Equip. **477**, 540 (2002).
[36] Mercurydpm.org.
[37] A. Thornton, T. Weinhart, S. Luding, and O. Bokhove, Int. J. Modern Phys. C **23**, 1240014 (2012).
[38] A. Thornton, T. Weinhart, V. Ogarko, and S. Luding, Comput. Methods Mater. Sci. **13**, 197 (2013).
[39] A. R. Thornton, D. Krijgsman, A. te Voortwis, V. Ogarko, S. Luding, R. Fransen, S. Gonzalez, O. Bokhove, O. Imole, and T. Weinhart, *DEM 6: Proceedings of the 6th International Conference on Discrete Element Methods and Related Techniques*, Vol. 393 (Colorado School of Mines, Colorado, 2013).
[40] P. A. Cundall and O. D. L. Strack, Geotechnique **29**, 47 (1979).
[41] S. Luding, Euro. J. Environ. Civ. Eng. **12**, 785 (2008).
[42] T. Weinhart, A. Thornton, S. Luding, and O. Bokhove, Granular Matter **14**, 531 (2012).
[43] M. P. Allen and D. J. Tildesley, eds., *Computer Simulation of Liquids* (Clarendon Press, Oxford, 1993).

[44] J. Mellmann, Powder Technol. **118**, 251 (2001).
[45] See Supplemental Material at http://link.aps.org/supplemental/10.1103/PhysRevE.92.022202 for animations of a selection of key simulations.
[46] M. B. Hu, X. Z. Kong, Q. S. Wu, and Y. H. Wu, Chinese Phys. B **14**, 1844 (2005).
[47] M. B. Hu, X. Z. Kong, Q. S. Wu, and Y. H. Wu, Int. J. Modern Phys. B **19**, 1793 (2005).
[48] D. Shi, A. A. Abatan, W. L. Vargas, and J. J. McCarthy, Phys. Rev. Lett. **99**, 148001 (2007).
[49] D. Mounty, Particle Size Segregation in Convex Rotating Drums, Ph.D. thesis (University of Manchester, 2007).
[50] M. Arntz, W. Den Otter, H. Beeftink, R. Boom, and W. Briels, Granular Matter **15**, 25 (2013).
[51] A. V. Orpe and D. V. Khakhar, Phys. Rev. E **64**, 031302 (2001).
[52] N. A. Pohlman, B. L. Severson, J. M. Ottino, and R. M. Lueptow, Phys. Rev. E **73**, 031304 (2006).
[53] Y. Fan and K. M. Hill, Phys. Rev. E **81**, 041303 (2010).
[54] S. E. Cisar, P. B. Umbanhowar, and J. M. Ottino, Phys. Rev. E **74**, 051305 (2006).
[55] S. J. Fiedor and J. M. Ottino, Phys. Rev. Lett. **91**, 244301 (2003).
[56] T. G. Townsend, J. Air Waste Manag. Assoc. **61**, 587 (2011).
[57] N. Mohabuth and N. Miles, Res. Conserv. Recycl. **45**, 60 (2005).
[58] N. Mohabuth, P. Hall, and N. Miles, Miner. Eng. **20**, 926 (2007).
[59] J. Gray and A. Thornton, Proc. R. Soc. A: Math. Phys. Eng. Sci. **461**, 1447 (2005).
[60] A. Thornton, J. Gray, and A. Hogg, J. Fluid Mech. **550**, 1 (2006).
[61] B. Marks, P. Rognon, and I. Einav, J. Fluid Mech. **690**, 499 (2012).
[62] Y. Fan and K. Hill, New J. Phys. **13**, 095009 (2011).
[63] K. Hill and D. S. Tan, J. Fluid Mech. **756**, 54 (2014).